Journal of Photochemistry & Photobiology, B: Biology 272 (2025) 113266

Contents lists available at ScienceDirect

Journal of Photochemistry & Photobiology, B: Biology

journal homepage: www.elsevier.com/locate/jphotobiol

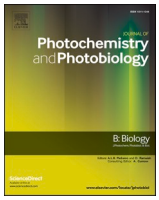

In situ sonoporation to enhance the tumour uptake of silicon phthalocyanine and improve PDT effectiveness in a triple negative breast cancer murine model

Martina Capozza [a], Alberto Mangia [a], Michela Gagliardi [a], Rachele Stefania [b], Francesca Garello [a], Laura Conti [a], Enzo Terreno [a,*]

[a] Department of Molecular Biotechnology and Health Sciences, University of Turin, Turin, Italy
[b] Department of Science and Technological Innovation, Università del Piemonte Orientale, Viale Teresa Michel 11, Alessandria, Italy

ARTICLE INFO

Keywords:
Sonoporation
Drug release
Photodynamic therapy
Breast cancer
NIRF imaging
Phthalocyanine

ABSTRACT

The effectiveness of photodynamic therapy (PDT) has been well demonstrated *in vitro*, but *in vivo* studies have only shown a delay in tumour growth. Tumour recurrence is often reported in clinical trials and is usually associated with limited tumour uptake of the photosensitiser (PS). In this study, sonoporation (SNP) is utilised as a physical targeting tool to enhance the uptake of an untargeted PS in cells and tumour tissues. Using a chemometric approach, we identified the optimal sonoporation stimulus to maximise uptake and cell viability (frequency 1.05 MHz, tON (percentage of positive signal in a single pulse): 50 %, DC: 90 %, burst: 1 s, sonoporation time 1 min). We achieved a viability of 83.9 % ± 10.3, and an uptake in live cells of 53.1 % ± 6.6. The combination of sonoporation and photodynamic therapy resulted in a significant reduction in cell viability. In a triple-negative breast cancer model, sonoporation combined with photodynamic therapy significantly inhibited tumour growth. For the first time, our results highlight the potential of sonoporation as a non-invasive method to increase the intratumour uptake of photosensitisers, offering a promising strategy to improve PDT efficacy.

1. Introduction

Breast cancer is the most commonly diagnosed cancer in women and the leading cause of cancer-related death [1]. Treatment of non-metastatic breast cancer typically involves surgical removal of the tumour and axillary lymph nodes [2]. The recurrence rate within the first 5 years after surgery is approximately 10 % [3]. However, for triple-negative breast carcinomas, this rate can increase as much as 50 % [4]. Positive or close pathological margins after breast-conserving surgery are associated with a higher risk of recurrence [5].

Photodynamic therapy (PDT) is based on the absorption of light by a photosensitiser (PS) at a specific wavelength, which activates the production of Reactive Oxygen Species (ROS) in the illuminated area [6–8]. Upon absorbing a photon, a photosensitiser (PS) reaches a singlet excited state (S1), from which it can transition to a triplet excited state (T1) through an intersystem crossing mechanism. The return to the ground state from the T1 level may proceed through various pathways, including the generation of free radicals (*e.g.*, O_2^-) or singlet oxygen ($^1O_2$). [9]. The advantage of photodynamic therapy (PDT) lies in its localised action: although a photosensitiser (PS) may distribute throughout other organs, it becomes toxic only when activated by precisely targeted laser irradiation. Additionally, depending on the central metal ion, the PS has a fluorescence that makes it available as a fluorescent dye. Its biodistribution and tumour accumulation can be monitored *in vivo* using optical imaging.

While PDT has often demonstrated strong efficacy *in vitro*, *in vivo* studies have shown only a delay in tumour growth [10–13]. Tumour recurrence is frequently observed in clinical trials, often due to limited PS uptake in the tumour tissue [14]. Recent advances aim to overcome this limitation by developing more selective and effective targeting moieties, which are directly attached to the PS or its delivery system [14–17].

In this study, we propose for the first time the use of sonoporation (SNP) as a physical targeting tool to promote the tumour uptake of an untargeted PS. Sonoporation uses ultrasounds (US) to induce transient pore formation in the plasma membrane, thereby locally improving drug uptake [18]. When ultrasound waves propagate through a fluid containing cells, the cells are subject to forces that increase membrane

* Corresponding author at: Department of Molecular Biotechnology and Health Sciences, University of Turin, Piazza Nizza 44bis, Turin, Italy.
E-mail address: enzo.terreno@unito.it (E. Terreno).

https://doi.org/10.1016/j.jphotobiol.2025.113266
Received 2 May 2025; Received in revised form 22 August 2025; Accepted 11 September 2025
Available online 12 September 2025

stress, leading to the formation of pores on the cell membrane [19,20]. In most applications, gas-core microbubbles (MBs) are intravenously injected to amplify the SNP effect by the occurrence of cavitation-induced processes [21–23]. Non-bubble based sonoporation is a novel approach developed to address the challenges associated with microbubble-enhanced sonoporation, such as the administration of MBs and reduced cell viability [19]. Although this approach has already been applied *in vitro* to enhance drug uptake in cell culture [19], few studies are reporting on non-bubble based sonoporation for drug delivery in tumour-bearing mice [24]. In contrast, sonoporation with the administration of microbubbles has been employed in preclinical tumour models [25,26]. Since sonoporation may alter membrane structure, it may be fatal to cells. While some cells attempt to restore homeostasis after membrane resealing, many ultimately fail to recover [27–29]. Therefore, to optimise ultrasound conditions for maximising PS uptake and cell viability, we applied a chemometric approach [30].

Herein, we investigated the cellular uptake of two PS based on phthalocyanine structure: $ZnPcS_4$, which is commercially available, and $SiPcS_4$, which was synthesised in-house, as well as their phototherapeutic efficacy *in vitro*. Then, we evaluated the sonoporation-mediated PS uptake and subsequent tumour volume reduction following light application in a triple-negative breast cancer mouse model.

2. Materials and methods

2.1. $SiPcS_4$ synthesis

All reagents were purchased from Sigma Aldrich (St. Louis, MO, USA) and were used without further purification. $SiPcS_4$ was synthesised following a previously reported procedure [31] (see supporting information).

2.2. Cell culture

K562 lymphoblastic cells and 4 T1 breast cancer cells were obtained from ATCC. Both K562 and 4 T1 were cultured in RPMI (Euroclone, Milan, Italy) supplemented with glutamine (2 mM), 10 % fetal bovine serum (Sigma-Aldrich, St. Louis, MO, USA) and penicillin/streptomycin antibiotics (10,000 IU/mL penicillin, 10,000 IU/mL streptomycin, Corning Cellgro, Manassas, VA, USA).

2.3. Photosensitiser characterization

Water-soluble, Zn(II)-phthalocyanine tetrasulfonic acid was obtained from eMolecules, Inc. (San Diego, CA). Excitation and emission spectra were measured using a FluoroMax-40 spectrofluorometer (Horiba Jobin Yvon, New York, NY). Samples at a concentration of 0.1 μM in Hank's Balanced Salt Solution (HBSS, Sigma-Aldrich, St. Louis, MO, USA) were excited by a 150 W Xenon light source and the fluorescence signal was detected using a TBX-04 detector. Emission spectra (λ_{exc} = 650 nm) were recorded between 660 nm and 800 nm, while excitation spectra (λ_{em} = 700 nm) were recorded between 550 nm and 690 nm. Both excitation and emission slits were set at 4 nm.

Absorbance spectra were measured using a Jenway 6715 UV/Visible Spectrophotometer (Cole Parmer, USA). To measure singlet oxygen generation, 9,10-Anthracenedipropanoic acid (ADPA) was purchased from Chemodex (Switzerland). 10 μL of ADPA (1 mg/mL in methanol) was added to 1 mL of phthalocyanine solution (2.5 μM in HBSS). The phthalocyanines were irradiated (λ = 660 nm, 160 mW/cm^2) at different timepoints (0–10 min). Absorbance spectra were acquired immediately after, and absorbance at 398 nm was plotted over irradiation time.

2.4. In vitro sonoporation

For the sonoporation experiments, the experimental setup followed the method described by Foglietta *et al* [32]. Briefly, 4×10^5 cells were pipetted into a polystyrene tube containing 1 mL of the drug (Carboxyfluorescein 50 μM, or $ZnPcS_4$ 30 μM or $SiPcS_4$ 1 μM). Ultrasound was generated using a plane wave transducer (with a diameter of 2.5 cm), operating in pulsed mode at a frequency of 1 MHz, that was combined to a power amplifier (Type 350 L 50 W, 250 kHz-150 MHz RF Amplifier; Electronics and Innovation, LTD, Rochester, NY, USA) and a function generator (Type 33500b; Keysight, USA). FACS polystyrene tubes containing cell suspension were inserted in a custom-built mechanical adaptor filled with ultrapure degassed water (a picture of the experimental setup is reported in Fig. S6). At the end of sonoporation, cells were incubated for 2 h at 4 °C, washed twice with PBS and resuspended in FACS buffer (2 % BSA, EDTA 1 mM in PBS). Propidium iodide (Sigma Aldrich, St. Louis, MO, USA) was added to assess cell viability, and samples were analysed using a BDFACSVerse® instrument (BD, New Jersey, USA). For the experiments with carboxyfluorescein, a 488 nm laser and 530/40 nm emission filter were used, while for $ZnPcS_4$, a 663 nm laser with an emission filter 750-long pass was used. 10^4 live cells/tube were acquired. Samples were analysed with BDFACSSuite and with FlowJO10.5.3 software.

2.5. Experimental design

Chemometric software CAT (Chemometric Agile Tool, *R. Leardi, C. Melzi, G. Polotti, CAT (Chemometric Agile Tool), freely downloadable from* http://gruppochemiometria.it/index.php/software) was used to plan the optimisation experiments to maximise cell viability and drug uptake. Full details of the experimental design are provided in the supplementary material.

2.6. Confocal microscopy

After sonoporation and PBS washing, 4 T1 cells were seeded into μ slide 8-well (ibidi GmbH, 82166 Gräfelfing, Germany) at a density of 2×10^5 cells per well. After 4 h, the cells were incubated with LysoTracker Green DND-26 (Invitrogen) at a final concentration of 100 nM for 10 min. Cells were then washed with PBS, fixed with 4 % paraformaldehyde (PAF) in PBS for 10 min. The day after, cells were permeabilised with 0.1 % Triton X-100 in PBS, and treated with DAPI (Sigma-Aldrich, St. Louis, MO, USA) 1:1000 for 20 min. Observations were made using a Leica TCS SP5 confocal microscope equipped with an argon ion. $SiPcS_4$ was visualised using a 633 nm laser, and DAPI was imaged using a 488 nm laser.

2.7. In vitro photodynamic therapy

K562 cells (1×10^6) were incubated with $ZnPcS_4$ or $SiPcS_4$ and sonoporated using the optimised parameters. After sonoporation, cells were incubated for 2 h at 4 °C, washed twice with PBS and then 5×10^5 K562 cells were seeded into 96-well plates. Cells were irradiated for 13 min at room temperature using a 90 mW lamp (λ = 660 nm) with a total energy dose of 70 J/cm^2. Cell viability was quantified 24 h post-irradiation using MTT (3-(4,5-dimethyl-2-thiazole)-2,5-diphenyl-2H-tetrazolium bromide; Sigma-Aldrich, St. Louis, MO, USA) assay. For controls, cells were sonoporated without irradiation (SNP+ PDT-) or irradiated without sonoporation (SNP- PDT+).

2.8. Animals

All institutional and national guidelines for the care and use of laboratory animals were followed (L.D. 26/2014; Directive 2010/63/EU) and under the approval of the Italian Ministry of Health (authorisation #298/2022). Mice were kept in standard housing with standard rodent chow and water available *ad libitum*, and a 12 h light/dark cycle. In order to perform tumour inoculation, sonoporation, PDT and imaging, mice were anaesthetised by intramuscular injection of a combination of

20 mg/kg tiletamine/zolazepam (Zoletil 100; Virbac, Milan, Italy) and 5 mg/kg xylazine (Rompun; Bayer, Milan, Italy).

2.9. $SiPcS_4$ tumour uptake and biodistribution

Female BALB/c mice (Envigo RMS, S.r.l., Udine, Italy) were subcutaneously injected with 6×10^4 4 T1 cells into both mouse flanks ($n = 8$ mice) under anaesthesia. Ten days post-tumour implantation, all mice were catheterised and intravenously administered with 20 nmol of $SiPcS_4$ while simultaneously tumours were sonoporated with the same parameters as used *in vitro*. Six mice were imaged by Near InfraRed Fluorescence (NIRF) imaging 4 h and 24 h after sonoporation using an IVIS Spectrum Instrument (Perkin Elmer, Shelton, USA), equipped with a CCD camera ($\lambda_{exc} = 640$ nm, $\lambda_{em} = 720$ nm). After imaging, mice were sacrificed, and organs were harvested to detect the fluorescence signal.

The remaining two mice were deeply anaesthetised 4 h after sonoporation and transcardially perfused with saline buffer 0.9 %. Tumours were then excised, embedded in optical cutting temperature (OCT) compound and snap-frozen in liquid nitrogen vapour. Tissue sections, 5 μm thick, were cut and fixed in 4 % PAF solution in PBS for 15 min. For immunofluorescence experiments, tissue sections were permeabilised with 0.1 % Triton X-100 in PBS for 10 min, saturated in 5 % normal goat serum (NGS) in PBS for 1 h and incubated with a rat monoclonal anti-CD31 (557355 BD Pharmingen, Milano, Italy) for 45 min at room temperature. An anti-rat Alexa Fluor 488 antibody (Molecular Probes, Invitrogen, Eugene, Oregon, USA), diluted 1:500, was used to detect the primary antibodies. For nuclear staining, the sections were treated with DAPI (Sigma-Aldrich, St. Louis, MO, USA) at a 1:1000 dilution for 20 min. Imaging was performed using a Leica TCS SP5 confocal microscope, as described above.

2.10. In vivo photodynamic therapy

Female BALB/c mice (Envigo RMS, S.r.l., Udine, Italy) were used for the study. Tumours were induced as described above. Ten days after tumour implantation (tumour volume of 30 ± 5 mm^3), mice were divided into different groups. Mice receiving both sonoporation and photodynamic therapy (SNP+ PDT+) were administered 20 nmol of $SiPcS_4$ and sonoporated. 4 h later, the tumour region was irradiated for 15 min at room temperature using a 90 mW lamp ($\lambda = 660$ nm, total light dose 160 J/cm^2). Controls included mice receiving only PDT (administered with 20 nmol of $SiPcS_4$ and irradiated 4 h p.i.), only sonoporation (administered with 20 nmol of $SiPcS_4$ and sonoporated simultaneously), or neither treatment. Two tumours were excluded from the study because of altered dimensions.

Tumour volumes were measured on day 0, 1, 3, 8, 11 and 15 post-treatment using a 7 T Bruker Pharmascan (Bruker Biospin, Ettlingen, Germany) MRI scanner equipped with a 30 mm 1H quadrature coil. Before imaging, mice were anaesthetised. T2 weighted (T2w) axial images were acquired with the following parameters: Echo time (TE) = 33 ms, Repetition Time (TR) = 2500 ms, Number of Averages = 2, matrix size = 256 × 256, Field of View (FOV) = 35 × 35 mm, slice thickness = 0.8 mm, acquisition time = 2 min and 40 s. Tumour volumes were calculated as the sum of tumour areas measured by manual outlining on every slice of the T2-weighted datasets, multiplied by the slice thickness.

2.11. Statistical analysis

Due to the relatively small sample size, differences in tumour growth rate between the treatment groups and the control group were compared with the non-parametric Kruskal-Wallis test for each time point. A *p*-value below 0.05 was considered significant.

3. Results and discussion

3.1. Photophysical properties of the photosensitisers

Synthesis and analytical characterization of $SiPcS_4$ are reported in the supplementary materials. The photophysical properties of zinc and silicon phthalocyanine tetrasulfonates ($ZnPcS_4$ and $SiPcS_4$, Fig. 1) were compared. Phthalocyanines are known for their strong absorption in the visible region and their ability to generate reactive oxygen species, making them ideal photosensitisers for photodynamic therapy (PDT). [33]

The spectral properties of $ZnPcS_4$ and $SiPcS_4$ were measured in HBSS (Fig. 2A and B). The excitation spectrum of $ZnPcS_4$ shows a maximum peak at 674 nm, while the emission spectrum has a maximum peak at 684 nm (10 nm Stokes shift). Similarly, the excitation spectrum of $SiPcS_4$ shows a maximum peak at 674 nm with the emission spectrum peaking at 683 nm (9 nm Stokes shift). These results suggest that the different central atoms in these phthalocyanines do not affect the fluorescence wavelength.

A critical property of photodynamic drugs is the generation of singlet oxygen ($^1O_2$), which plays a key role in cytotoxicity during PDT. ADPA was used as a singlet oxygen quencher, and the decay of ADPA's absorption band at 398 nm was monitored as a function of the irradiation time using UV–vis spectrophotometry. [34,35] As illustrated in Fig. 2C and D, the absorbance of ADPA in solutions containing phthalocyanines decreases with irradiation time (irradiation power 160 mW/cm^2). Notably, the absorbance declines more rapidly with silicon phthalocyanine, suggesting that $SiPcS_4$ has a greater capacity to generate $^1O_2$. [36]

3.2. SNP optimisation by chemometry (D-optimal)

To maximise cellular drug uptake and cellular viability, an experimental design approach (D-optimal design) [37] was applied (see supplementary material), incubating cells with drugs (*i.e.* carboxyfluorescein for optimisation in Figs. S7–S11 and $ZnPcS_4$ in Figs. S12–S13). The optimal sonoporation conditions, which achieved the best balance between cellular uptake and cell viability, were US frequency 1.05 MHz, tON 50 %, DC90%, burst duration 1 s and a total exposure time of 1 min. Under these conditions (sample n° 17 in Fig. S12), the cell viability was 83.9 % ± 10.3, with 53.1 % ± 6.6 of live cells being positively stained, and an MFI value of 4095 ± 1120. These findings are in agreement with data already reported in the literature [38]. Temperature rise during ultrasound application can significantly influence therapeutic effects [39]. For this reason, temperature has been monitored, showing a limited temperature increase up to 10 min of sonoporation. (Fig. S14).

Fluorescence confocal microscopy confirmed the presence of $SiPcS_4$ in sonoporated cells. As indicated by the white arrow in Fig. 3B, some cell debris showed phthalocyanine uptake. Additionally, the intracellular localisation of $SiPcS_4$ within lysosomes was observed.

Flow cytometry (Fig. 3C) and fluorescence confocal microscopy experiments indicated that sonoporation enhanced the intracellular delivery of different molecules. The optimal ultrasound conditions identified in these experiments could be utilised in future studies to maximise the therapeutic potential of sonoporation in combination with different photosensitisers or drugs.

3.3. Photodynamic therapy in vitro

Cells are sonoporated as previously described (US frequency 1.05 MHz, tON 50 %, DC90%, burst duration 1 s and a total exposure time of 1 min). PDT experiments using $ZnPcS_4$ (Fig. 4A and B) showed a decrease in cell viability when cells were both sonoporated and irradiated, with viability reduced to 20 % at 30 μM and 60 % at 1 μM $ZnPcS_4$. In contrast, when cells were not sonoporated, the PDT effect was

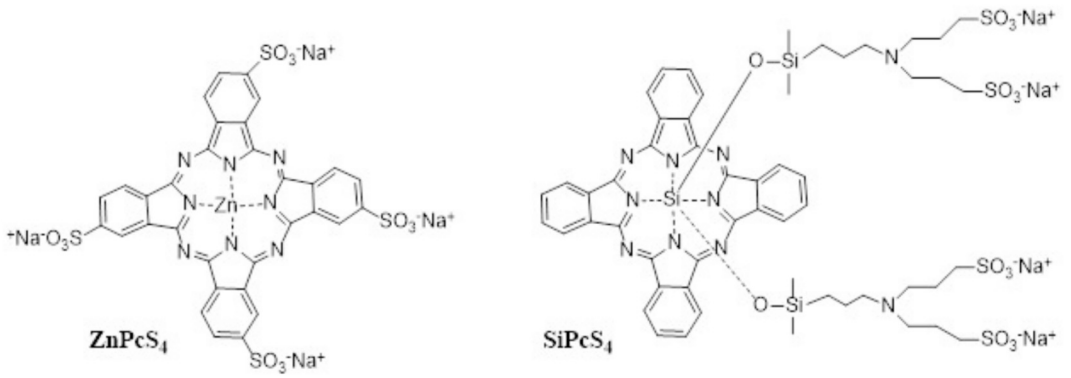

Fig. 1. Chemical structure of $ZnPcS_4$ and $SiPcS_4$.

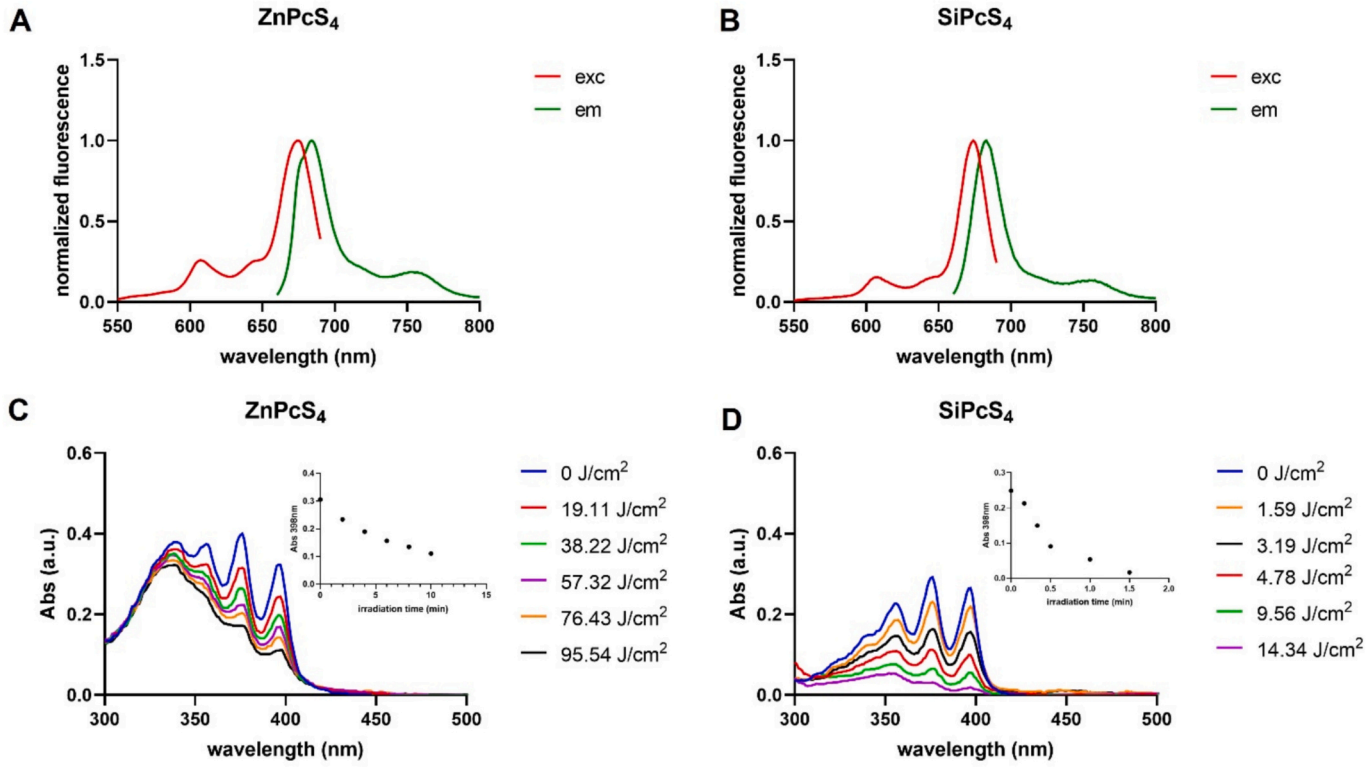

Fig. 2. Excitation and emission spectra of $ZnPcS_4$ (A) and $SiPcS_4$ (B); Absorbance spectra after different irradiation times ($\lambda = 660$ nm; 160 mW/cm^2) of ADPA and $ZnPcS_4$ (C) and $SiPcS_4$ (D).

significantly weaker, with viability at 82 % for 30 μM and 95 % for 1 μM $ZnPcS_4$. Similar results were obtained with $SiPcS_4$ (Fig. 4C). Although $SiPcS_4$ does not generate singlet oxygen upon sonoporation (Fig. S15), even the sonoporated but non-illuminated samples exhibited low viability (approximately 40 %). Despite this, the combination of SNP and PDT with 1 μM $SiPcS_4$ proved highly effective, reducing cell viability to 30 %.

The difference observed between $ZnPcS_4$ and $SiPcS_4$ at 1 μM suggests that $SiPcS_4$ is much more efficient as a PDT agent compared to $ZnPcS_4$, as confirmed by singlet oxygen generation (Fig. 2C and D). A statistical comparison (*t*-test) between SNP+/PDT+ and SNP+/PDT- experiments highlighted that, in the case of $ZnPcS_4$ (at 1 μM), illumination did not have a significant effect on cell viability. In contrast, for $SiPcS_4$, a *p*-value of 0.0022 was calculated, further confirming that $SiPcS_4$ is a more potent photosensitiser than $ZnPcS_4$.

However, the data also revealed a certain level of cytotoxicity in all SNP+/PDT- samples, which seems correlated to the PS concentration. Since sonoporation alone does not fully account for this observation, this effect may likely arise from a sonodynamic effect induced by the PS, as recently reported for silicon phthalocyanines. [40] This could be an interesting finding for future research, as the sonophotodynamic approach could reduce the dose of ultrasound, light and sensitisers, maximising efficacy while reducing side effects. [41–43]

3.4. NIRF imaging: tumour uptake and biodistribution of $SiPcS_4$

20 nmol of $SiPcS_4$ were intravenously administered to 4 T1 tumour-bearing mice and, simultaneously, one of the two tumours was sonoporated (US frequency 1.05 MHz, tON 50 %, DC90%, burst duration 1 s and a total exposure time of 1 min). Mice were imaged by NIRF imaging 4 h and 24 h post-treatment, after which they were sacrificed, and their organs excised. At the 4-h time point, liver, kidneys, lungs, and sonoporated tumour (TUM SNP) displayed the strongest fluorescence, while the control tumour exhibited a weaker signal. Notably, skin fluorescence

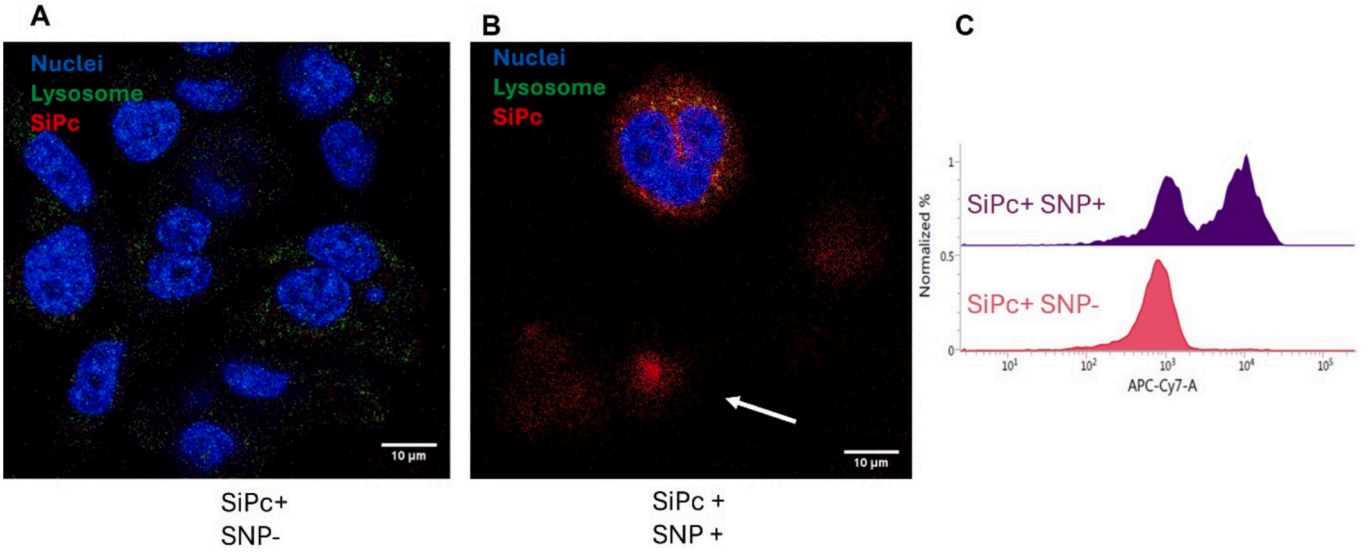

Fig. 3. Confocal images of 4 T1 cell line after incubation (A) and incubation and sonoporation with $SiPcS_4$ (B), $SiPcS_4$ is in red, DAPI for nuclei visualisation in blue and LysoTracker for lysosome in green. The white arrow indicates cell debris exhibiting phthalocyanine signal. (C) Representative flow cytometry of incubated and sonoporated 4 T1 cells (upper panel) or incubated 4 T1 cells (lower panel). (For interpretation of the references to colour in this figure legend, the reader is referred to the web version of this article.)

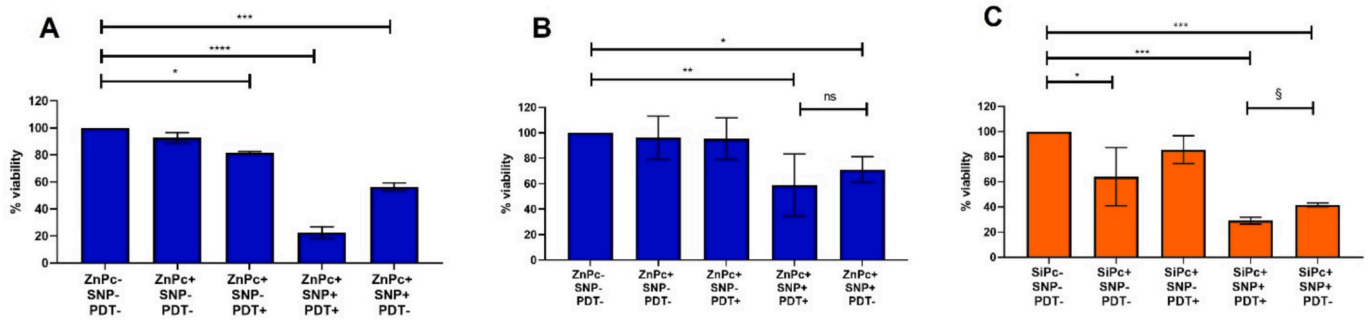

Fig. 4. Viability of cells 24 h post irradiation (70 J/cm^2) and incubation with 30 µM of $ZnPcS_4$ (A), 1 µM of $ZnPcS_4$ (B) and 1 µM of $SiPcS_4$ (C). Each data point represents the mean ± SD of three independent experiments. * $p < 0.05$, ** $p < 0.001$ and *** $p < 0.0001$ 2-way ANOVA repeated measures followed by Bonferroni *post hoc* test. § $p = 0.0022$ *t*-test.

remained consistently very low, which is crucial for minimising photodynamic therapy side effects such as skin hypersensitivity to light, which can last for several weeks [44].

Although sonoporated tumours exhibited a higher Tumour-to-Muscle ratio (TMR) at 24 h (Fig. 5C), the maximum accumulation of the photosensitiser (PS) in the tumour, which is critical for its therapeutic effect [32], was observed 4 h post sonoporation. Consequently, this time point was selected for the PDT treatment.

Fluorescence confocal microscopy of tumour tissue, perfused 4 h post-$SiPcS_4$ administration with or without sonoporation, confirmed the biodistribution results. The $SiPcS_4$ signal was only detectable in sonoporated tumours (Fig. 5E and F). CD31 staining was performed to visualise the vascular structure, but it was barely observed in sonoporated tumours (Fig. 5E and F). However, it has been previously reported that especially immature tumour vasculature is subject to endothelium damage and depletion after sonoporation [45,46].

Among all, near-infrared fluorescence (NIRF) imaging showed that $SiPcS_4$ accumulated preferentially in sonoporated tumours compared to untreated tumours. This is an innovative approach because, for the first time, sonoporation is performed to increase the "passive" uptake of a small molecule without the administration of microbubbles *in vivo* [47–49], and without the use of a tumour-targeted PS.

3.5. Photodynamic therapy in vivo

For the *in vivo* photodynamic therapy study, 4 T1 tumour-bearing mice were intravenously administered with 20 nmol $SiPcS_4$ and one of the two tumours was sonoporated during the injection. Four hours later, the tumour region was illuminated with a light dose of 160 J/cm^2. Tumour volume was monitored using T_{2w}-MRI for 15 days (Fig. 6). The results showed that the combination of SNP and PDT significantly inhibited tumour growth. In contrast, neither sonoporation nor laser irradiation alone had a significant effect.

In 2020, the first clinical study of PDT in the treatment of primary breast cancer was published. In this study, the photosensitiser (PS) was administered intravenously, and light energy was delivered directly to the tumour *via* a fiber laser, highlighting PDT's potential role in breast cancer management [50]. Since our approach is untargeted, the same untargeted PS could in principle be applied to various cancers. Additionally, advancements in endoscopy-based techniques that combine ultrasound and laser technology may further broaden PDT's application to gastrointestinal cancers. [51]

4. Conclusion

In this study, we demonstrated that silicon phthalocyanine

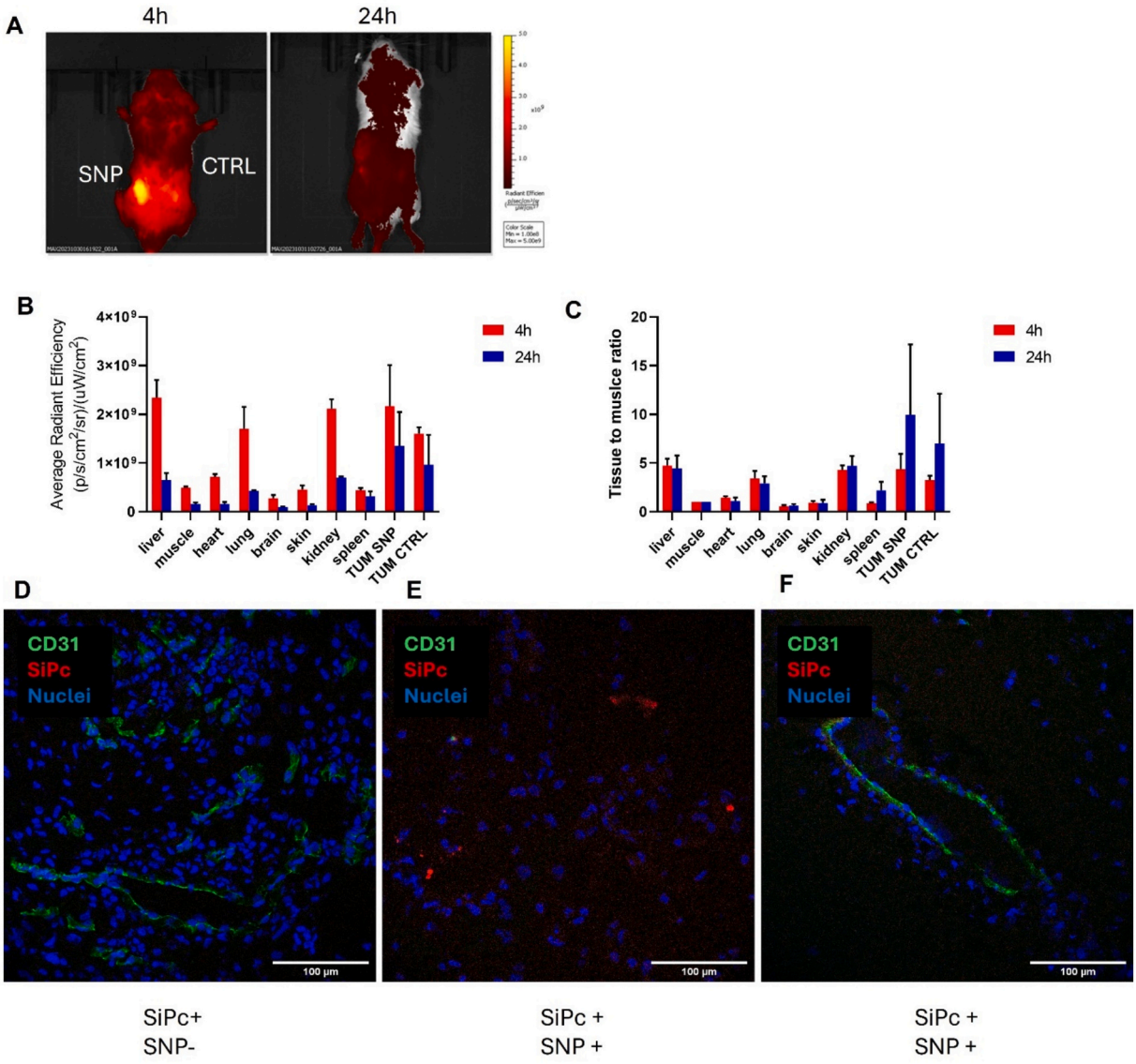

Fig. 5. *In vivo* optical images of 4 T1-tumour bearing mice 4 h and 24 h after administration and sonoporation of 20 nmol of $SiPcS_4$ ($n = 3$ group), λexc = 640 nm (30 nm bandwidth), λem = 720 nm (20 nm bandwidth); A) representative images; B) *Ex vivo* optical imaging of different organs after 20 nmol administration; C) Signal intensity ratios calculated between different organs and the muscle region at various time points post-injection; D) Confocal fluorescence images of 4 T1 tumours administered with $SiPcS_4$ but not sonoporated (SiPc+ SNP-); E) and F) Confocal fluorescence images of 4 T1 tumours administered with $SiPcS_4$ and sonoporated (SiPc+ SNP+).

tetrasulfonate ($SiPcS_4$) is a more effective photosensitiser than zinc phthalocyanine tetrasulfonate ($ZnPcS_4$) in the context of photodynamic therapy (PDT). The enhanced singlet oxygen generation and cytotoxicity of $SiPcS_4$, combined with sonoporation, significantly inhibited tumour growth *in vivo*. Our results highlight the potential of sonoporation as a non-invasive method to increase the intratumour uptake of photosensitisers, offering a promising strategy to improve PDT efficacy. Likely, $SiPcS_4$ also exhibited sonodynamic effects, reducing cell viability even in the absence of illumination, which suggests a dual therapeutic mechanism involving both ultrasound and light.

While the use of sonoporation to enhance drug delivery without microbubbles represents a novel approach, further studies are needed to explore the clinical implications of the observed sonodynamic effects and to optimise this strategy for broader cancer treatments. However, this study has several limitations. One key limitation is the poor translatability of the animal model to human clinical scenario, as animal tumour models (especially subcutaneous tumours) may not fully replicate the complexity of human tumours, including differences in tumour microenvironment, immune response, and drug metabolism. Although tumour growth was reduced, complete suppression was not achieved. This suggests that further optimisation of the treatment regimen—such as adjusting the photosensitiser dosage, adjusting light exposure parameters, or combining the therapy with other treatment modalities—may be necessary to enhance therapeutic efficacy. It could also be interesting to evaluate how sonoporation affects normal cells, to study whether there is selective membrane permeability in cancer *versus* normal cells [52].

Despite the limitations related to tumour suppression and the use of animal models, our findings open new avenues for combining sonoporation with photosensitisers, which could reduce the required doses of ultrasound, light, and sensitisers, ultimately improving therapeutic outcomes while minimising side effects. Furthermore, the use of an untargeted PS may bypass the need for synthesising targeted agents, which can be complex and may suffer from poor water solubility and optimisation of their biodistribution. This study lays the groundwork for future research into sonophotodynamic therapy and its potential clinical

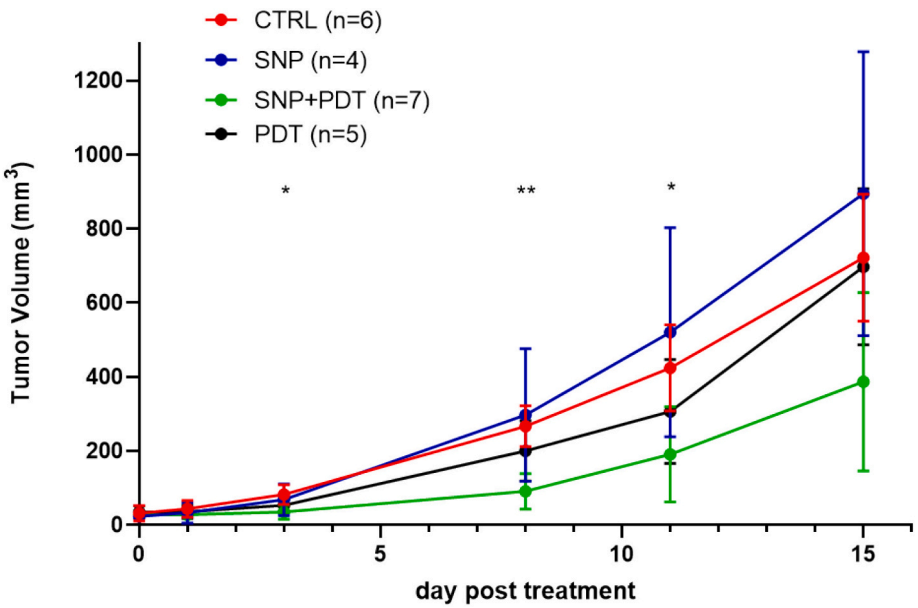

Fig. 6. Tumour volume dimension measured *via* MRI after treatment. * $p < 0.05$ and ** $p < 0.001$ Kruskal-Wallis test CTRL *vs* SNP + PDT.

applications in cancer treatment.

Author contribution

All authors contributed to the study conception and design. Material preparation, data collection and analysis were performed by Martina Capozza, Michela Gagliardi, Alberto Mangia and Enzo Terreno. The first draft of the manuscript was written by Martina Capozza and all authors commented on previous versions of the manuscript. All authors read and approved the final manuscript.

CRediT authorship contribution statement

Martina Capozza: Writing – original draft, Data curation, Conceptualization. **Alberto Mangia:** Methodology. **Michela Gagliardi:** Software, Data curation. **Rachele Stefania:** Data curation. **Francesca Garello:** Supervision, Methodology. **Laura Conti:** Supervision, Methodology. **Enzo Terreno:** Writing – review & editing, Funding acquisition.

Consent for publication

All authors have approved the final version of the manuscript.

Ethics approval

All institutional and national guidelines for the care and use of laboratory animals were followed.

Funding

This work was supported by Associazione Italiana per la Ricerca sul Cancro (AIRC, Grant number IG-22041) and the FOE to Euro-BioImaging Multi-Modal Molecular Imaging Italian Node (MMMI).

Declaration of competing interest

The authors have no relevant financial or non-financial interests to disclose.

Acknowledgements

We thank Dr. Valeria Bitonto for her assistance with confocal images acquisition.

Appendix A. Supplementary data

Supplementary data to this article can be found online at https://doi.org/10.1016/j.jphotobiol.2025.113266.

Data availability

Data will be made available on request. All data are provided in the manuscript and supplementary fle.

References

[1] R.L. Siegel, A.N. Giaquinto, A. Jemal, Cancer statistics, 2024, CA Cancer J. Clin. 74 (2024) 12–49.
[2] M. Akram, M. Iqbal, M. Daniyal, A.U. Khan, Awareness and current knowledge of breast cancer, Biol. Res. 50 (2017) 33.
[3] M. Colleoni, Z. Sun, K.N. Price, P. Karlsson, J.F. Forbes, B. Thürlimann, et al., Annual Hazard rates of recurrence for breast cancer during 24 years of follow-up: results from the international breast cancer study group trials I to V, J. Clin. Oncol. 34 (2016) 927–935.
[4] R.L.B. Costa, W.J. Gradishar, Triple-negative breast cancer: current practice and future directions, J. Oncol. Pract. 13 (2017) 301–303.
[5] J.R. Bundred, S. Michael, B. Stuart, R.I. Cutress, K. Beckmann, B. Holleczek, et al., Margin status and survival outcomes after breast cancer conservation surgery: prospectively registered systematic review and meta-analysis, BMJ 378 (2022) e070346.
[6] D. Aebisher, J. Szpara, D. Bartusik-Aebisher, Advances in medicine: photodynamic therapy, Int. J. Mol. Sci. (2024) 25.
[7] P. Sarbadhikary, B.P. George, H. Abrahamse, Recent advances in photosensitizers as multifunctional theranostic agents for imaging-guided photodynamic therapy of cancer, Theranostics 11 (2021) 9054–9088.
[8] T.J. Dougherty, C.J. Gomer, B.W. Henderson, G. Jori, D. Kessel, M. Korbelik, et al., Photodynamic therapy, J. Natl. Cancer Inst. 90 (1998) 889–905.
[9] H. Jin, S. Liao, F. Yao, J. Li, Z. Xu, K. Zhao, et al., Insight into the crosstalk between photodynamic therapy and immunotherapy in breast cancer, Cancers (Basel) (2023) 15.
[10] Y.H.W. Derks, M. Rijpkema, H.I.V. Amatdjais-Groenen, A. Kip, G.M. Franssen, J.P. M. Sedelaar, et al., Photosensitizer-based multimodal PSMA-targeting ligands for intraoperative detection of prostate cancer, Theranostics 11 (2021) 1527–1541.
[11] Y.H.W. Derks, M.G.M. Schilham, M. Rijpkema, E.M.M. Smeets, H.I.V. Amatdjais-Groenen, A. Kip, et al., Imaging and photodynamic therapy of prostate cancer using a theranostic PSMA-targeting ligand, Eur. J. Nucl. Med. Mol. Imaging 50 (2023) 2872–2884.

[12] M. Capozza, R. Stefania, V. Dinatale, V. Bitonto, L. Conti, C. Grange, et al., A novel PSMA-targeted probe for NIRF-guided surgery and photodynamic therapy: synthesis and preclinical validation, Int. J. Mol. Sci. 23 (2022).
[13] X. Wang, J. Hu, P. Wang, S. Zhang, Y. Liu, W. Xiong, et al., Analysis of the in vivo and in vitro effects of photodynamic therapy on breast cancer by using a sensitiser, sinoporphyrin sodium, Theranostics 5 (2015) 772–786.
[14] J. Xie, Y. Wang, W. Choi, P. Jangili, Y. Ge, Y. Xu, et al., Overcoming barriers in photodynamic therapy harnessing nano-formulation strategies, Chem. Soc. Rev. 50 (2021) 9152–9201.
[15] X. Wang, D. Luo, J.P. Basilion, Photodynamic therapy: targeting cancer biomarkers for the treatment of cancers, Cancers (Basel) (2021) 13.
[16] M.B. Quaye, G. Obaid, Recent strides in macromolecular targeted photodynamic therapy for cancer, Curr. Opin. Chem. Biol. 81 (2024) 102497.
[17] V. Dinatale, M. Capozza, R. Stefania, S. Liuzzi, H.S. de Bruijn, R. McMorrow, et al., Exploring Si-phthalocyanines with different valency for PSMA-targeted photodynamic therapy: synthesis and preclinical validation, Eur. J. Med. Chem. 290 (2025) 117562.
[18] J. Tu, A.C.H. Yu, Ultrasound-mediated drug delivery: sonoporation mechanisms, biophysics, and critical factors, BME Front. 2022 (2022) 9807347.
[19] J. Rich, Z. Tian, T.J. Huang, Sonoporation: past, present, and future, Adv. Mater. Technol. (2022) 7.
[20] B. Han, Y. Liu, Q. Zhou, Y. Yu, X. Liu, Y. Guo, et al., The advance of ultrasound-enabled diagnostics and therapeutics, J. Control. Release 375 (2024) 1–19.
[21] B.D. Meijering, L.J. Juffermans, A. van Wamel, R.H. Henning, I.S. Zuhorn, M. Emmer, et al., Ultrasound and microbubble-targeted delivery of macromolecules is regulated by induction of endocytosis and pore formation, Circ. Res. 104 (2009) 679–687.
[22] B. van Elburg, J. Deprez, M. van den Broek, S.C. De Smedt, M. Versluis, G. Lajoinie, et al., Dependence of sonoporation efficiency on microbubble size: an in vitro monodisperse microbubble study, J. Control. Release 363 (2023) 747–755.
[23] M. Eck, R. Aronovich, T. Ilovitsh, Efficacy optimization of low frequency microbubble-mediated sonoporation as a drug delivery platform to cancer cells, Int. J. Pharm. X 4 (2022) 100132.
[24] S.M. Chowdhury, L. Abou-Elkacem, T. Lee, J. Dahl, A.M. Lutz, Ultrasound and microbubble mediated therapeutic delivery: underlying mechanisms and future outlook, J. Control. Release 326 (2020) 75–90.
[25] K. Iwanaga, K. Tominaga, K. Yamamoto, M. Habu, H. Maeda, S. Akifusa, et al., Local delivery system of cytotoxic agents to tumours by focused sonoporation, Cancer Gene Ther. 14 (2007) 354–363.
[26] O. Eikrem, S. Kotopoulis, M. Popa, M. Mayoral Safont, K.O. Fossan, S. Leh, et al., Ultrasound and microbubbles enhance uptake of doxorubicin in murine kidneys, Pharmaceutics (2021) 13.
[27] X. Duan, Q. Zhou, J.M.F. Wan, A.C.H. Yu, Sonoporation generates downstream cellular impact after membrane resealing, Sci. Rep. 11 (2021) 5161.
[28] D. Przystupski, M. Ussowicz, Landscape of cellular bioeffects triggered by ultrasound-induced sonoporation, Int. J. Mol. Sci. 23 (2022).
[29] J. Shi, Y. Ma, R. Shi, A.C.H. Yu, P. Qin, Manipulating long-term fates of sonoporated cells by regulating intracellular calcium for improving sonoporation-based delivery, J. Control. Release 375 (2024) 142–154.
[30] R.G. Brereton, J. Jansen, J. Lopes, F. Marini, A. Pomerantsev, O. Rodionova, et al., Chemometrics in analytical chemistry-part I: history, experimental design and data analysis tools, Anal. Bioanal. Chem. 409 (2017) 5891–5899.
[31] K. Sato, K. Ando, S. Okuyama, S. Moriguchi, T. Ogura, S. Totoki, et al., Photoinduced ligand release from a silicon phthalocyanine dye conjugated with monoclonal antibodies: a mechanism of cancer cell cytotoxicity after near-infrared photoimmunotherapy, ACS Cent. Sci. 4 (2018) 1559–1569.
[32] F. Foglietta, M. Macrì, P. Panzanelli, A. Francovich, G. Durando, F. Garello, et al., Ultrasound boosts doxorubicin efficacy against sensitive and resistant ovarian cancer cells, Eur. J. Pharm. Biopharm. 183 (2023) 119–131.
[33] P.C. Lo, M.S. Rodríguez-Morgade, R.K. Pandey, D.K.P. Ng, T. Torres, F. Dumoulin, The unique features and promises of phthalocyanines as advanced photosensitisers for photodynamic therapy of cancer, Chem. Soc. Rev. 49 (2020) 1041–1056.
[34] S. Kim, M. Fujitsuka, T. Majima, Photochemistry of singlet oxygen sensor green, J. Phys. Chem. B 117 (2013) 13985–13992.
[35] A. Gomes, E. Fernandes, J.L. Lima, Fluorescence probes used for detection of reactive oxygen species, J. Biochem. Biophys. Methods 65 (2005) 45–80.
[36] M. Capozza, G. Digilio, M. Gagliardi, L. Tei, S. Marchesi, E. Terreno, et al., Silicon phthalocyanines functionalized with axial substituents targeting PSMA: synthesis and preliminary assessment of their potential for photodynamic therapy of prostate cancer, ChemMedChem 19 (2024) e202400218, https://doi.org/10.1002/cmdc.202400218.
[37] Z. Gong, X. Zhu, C. Zhang, D-optimal design of the additive mixture model with multi-response, Math. Biosci. Eng. 19 (2022) 4737–4748.
[38] D. Shi, L. Guo, S. Duan, M. Shang, D. Meng, L. Cheng, et al., Influence of tumor cell lines derived from different tissue on sonoporation efficiency under ultrasound microbubble treatment, Ultrason. Sonochem. 38 (2017) 598–603.
[39] S.E.N. Price, M.A. Gjennestad, S. Kjelstrup, R. Hansen, The effect of temperature constraints on the treatment of tumors using focused ultrasound-induced acoustic streaming, Sci. Rep. 15 (2025) 49.
[40] G.G. Köse, A. Erdoğmuş, Dual effect of light and ultrasound for efficient singlet oxygen generation with novel diaxial silicon phthalocyanine sensitizer, Photochem. Photobiol. 100 (2024) 52–66.
[41] G.Y. Atmaca, M. Aksel, M.D. Bilgin, A. Erdoğmuş, Comparison of sonodynamic, photodynamic and sonophotodynamic therapy activity of fluorinated pyridine substituted silicon phthalocyanines on PC3 prostate cancer cell line, Photodiagn. Photodyn. Ther. 42 (2023) 103339.
[42] H. Messaoudi, G. Yaşa Atmaca, A. Türkkol, M.D. Bilgin, A. Erdoğmuş, Monitoring of singlet oxygen generation of a novel Schiff-base substituted silicon phthalocyanines by sono-photochemical studies and in vitro activities on prostate cancer cell, J. Biol. Inorg. Chem. 29 (2024) 303–314.
[43] L.C. Nene, H. Abrahamse, Design consideration of phthalocyanines as sensitizers for enhanced sono-photodynamic combinatorial therapy of cancer, Acta Pharm. Sin. B 14 (2024) 1077–1097.
[44] S. Kwiatkowski, B. Knap, D. Przystupski, J. Saczko, E. Kędzierska, K. Knap-Czop, et al., Photodynamic therapy - mechanisms, photosensitizers and combinations, Biomed. Pharmacother. 106 (2018) 1098–1107.
[45] J. Wang, Z. Zhao, S. Shen, C. Zhang, S. Guo, Y. Lu, et al., Selective depletion of tumor neovasculature by microbubble destruction with appropriate ultrasound pressure, Int. J. Cancer 137 (2015) 2478–2491.
[46] F. Padilla, J. Brenner, F. Prada, A.L. Klibanov, Theranostics in the vasculature: bioeffects of ultrasound and microbubbles to induce vascular shutdown, Theranostics 13 (2023) 4079–4101.
[47] P. Nittayacharn, E. Abenojar, M.B. Cooley, F.M. Berg, C. Counil, A.J. Sojahrood, et al., Efficient ultrasound-mediated drug delivery to orthotopic liver tumors - direct comparison of doxorubicin-loaded nanobubbles and microbubbles, J. Control. Release 367 (2024) 135–147.
[48] K.D. Watson, C.Y. Lai, S. Qin, D.E. Kruse, Y.C. Lin, J.W. Seo, et al., Ultrasound increases nanoparticle delivery by reducing intratumoral pressure and increasing transport in epithelial and epithelial-mesenchymal transition tumors, Cancer Res. 72 (2012) 1485–1493.
[49] T.Y. Wang, J.W. Choe, K. Pu, R. Devulapally, S. Bachawal, S. Machtaler, et al., Ultrasound-guided delivery of microRNA loaded nanoparticles into cancer, J. Control. Release 203 (2015) 99–108.
[50] S.M. Banerjee, S. El-Sheikh, A. Malhotra, C.A. Mosse, S. Parker, N.R. Williams, et al., Photodynamic therapy in primary breast cancer, J. Clin. Med. (2020) 9.
[51] Y. Yi, L. Li, J. Li, X. Shu, H. Kang, C. Wang, et al., Use of lasers in gastrointestinal endoscopy: a review of the literature, Lasers Med. Sci. 38 (2023) 97.
[52] R. Haugse, A. Langer, S.E. Gullaksen, S.M. Sundøy, B.T. Gjertsen, S. Kotopoulis, et al., Intracellular signaling in key pathways is induced by treatment with ultrasound and microbubbles in a leukemia cell line, but not in healthy peripheral blood mononuclear cells, Pharmaceutics (2019) 11.